The Regional Climate-Chemistry-Ecology Coupling Model RegCM-Chem (v4.6)-YIBs (v1.0): Development and Application

Nanhong Xie[1], Tijian Wang[1]*, Xiaodong Xie[2], Xu Yue[2], Filippo Giorgi[3], Qian Zhang[1], Danyang Ma[1], Rong Song[1], Beiyao Xu[1], Shu Li[1], Bingliang Zhuang[1], Mengmeng Li[1], Min Xie[1], Natalya Andreeva Kilifarska[4], Georgi Gadzhev[5], Reneta Dimitrova[6]

[1]School of Atmospheric Sciences, Nanjing University, Nanjing, 210023, China

[2]School of Environmental Sciences and Engineering, Nanjing University of Information Science and Technology, Nanjing, 210023, China

[3]Earth System Physics Section, the Abdus Salam International Centre for Theoretical Physic, Trieste, 34100, Italy

[4]Climate, Atmosphere and Waters Research Institute, Bulgarian Academy of Sciences, Sofia, 1113, Bulgaria

[5]National Institute of Geophysics, Geodesy and Geography, Bulgarian Academy of Sciences, Sofia, 1113, Bulgaria

[6]Department of Meteorology and Geophysics, Faculty of Physics, Sofia University, Sofia, 1113, Bulgaria

Corresponding to: Tijian Wang (tjwang@nju.edu.cn)

Abstract. The interactions between the terrestrial biosphere, atmospheric chemistry, and climate involve complex feedbacks that have traditionally been modeled separately. We present a new framework that couples the Yale Interactive terrestrial Biosphere (YIBs), a dynamic plant-chemistry model, with the RegCM-Chem model. RegCM-Chem-YIBs integrates meteorological variables and atmospheric chemical composition from RegCM-Chem with land surface parameters from YIBs. The terrestrial carbon flux calculated by YIBs, are fed back into RegCM-Chem interactively, thereby representing the interactions between fine particulate matter ($PM_{2.5}$), ozone (O_3), and carbon dioxide (CO_2). For testing purposes, we carry out a one-year simulation (2016) at a 30 km horizontal resolution over East Asia with RegCM-Chem-YIBs. The model accurately captures the spatio-temporal distribution of climate, chemical composition, and ecological parameters. In particular, the estimated O_3 and $PM_{2.5}$ are consistent with ground observations, with correlation coefficients (R) of 0.74 and 0.65, respectively. The simulated CO_2 concentration is consistent with observations from six sites (R ranged from 0.89 to 0.97) and exhibits a similar spatial pattern when compared to carbon assimilation products. RegCM-Chem-YIBs produces reasonably good gross primary productivity (GPP) and net primary productivity (NPP), showing seasonal and spatial distributions consistent with satellite observations, and mean biases (MBs) of 0.13 and 0.05 kg C m^{-2} year^{-1}. This study illustrates that the RegCM-Chem-YIBs is a valuable tool to investigate coupled interactions between the terrestrial carbon cycle, atmospheric chemistry, and climate change at a higher resolution in regional scale.

1 Introduction

Air pollution and climate change are major focal points in atmospheric and environmental science (Hong et al., 2019; Kan et al., 2012). In this respect, China exhibits both high air pollution levels and large greenhouse gas emissions (Zheng et al., 2018; Li et al., 2016a). The consequences of China's air pollution on global, regional, and urban climate are significant (Liu et al., 2022; Lu et al., 2020). Conversely, global warming impacts the dynamics, physics, and chemical mechanisms underlying atmospheric pollutant formation, underscoring a robust link between atmospheric chemistry and climate change (Baklanov et al., 2016; Fiore et al., 2015; Fiore et al., 2012).

$PM_{2.5}$, O_3, and CO_2 are important for regional air pollution and climate. O_3, a potent pollutant, is harmful for human health and can also harm chloroplasts in plant cells, consequently influencing the carbon assimilation efficiency of land ecosystems (Xie et al., 2019; Ainsworth et al., 2012). Similarly, $PM_{2.5}$ is not only one of the most dangerous pollutants for human health (Kim et al., 2015), but also affects atmospheric radiation mechanics, modulates radiation fluxes reaching vegetation canopies, and hence impacts plant physiological processes and terrestrial carbon fluxes (Lu et al., 2017; Strada and Unger, 2016). Terrestrial ecosystems, absorbing nearly 30% of anthropogenic CO_2 emissions, play an essential role in the global carbon cycle, for which even minor alterations can trigger significant oscillations in atmospheric CO_2 concentrations, potentially destabilizing the global climate (Forkel et al., 2016; Ahlstrom et al., 2015). As a result, $PM_{2.5}$, O_3, and CO_2 exhibit intricate interplays.

Models that couple climate and chemistry are vital tools for investigating the interplay between environmental pollution and climate warming (Dunne et al., 2020; Yahya et al., 2017), and in particular the direct and indirect influences of aerosols, O_3, and greenhouse gases on climates at different scales (Chutia et al., 2019; Pu et al., 2017; Li et al., 2017a). For example, the Atmospheric Chemistry and Climate Model Intercomparison Project (ACCMIP) addresses this issue through the use of a range of global coupled climate-chemistry models (Young et al., 2013; Shindell et al., 2013; Lamarque et al., 2013). In fact, China has achieved significant advancements in atmospheric chemistry and coupled climate models during recent years, both at the global and regional scale. Representative models encompass BCC_AGCM2.0_CAM, BCC-AGCM_CUACE2.0, RIEMS-Chem, and RegCCMS.

BCC_AGCM2.0_CAM was coupled by the China Meteorological Administration through direct integration of the National Climate Center's atmospheric circulation model (BCC-AGCM) with the Canadian aerosol model (CAM) (Zhang et al., 2012). Atmospheric model BCC-AGCM2.0 was developed by the National Climate

Center. For example, at the regional scale the Institute of Atmospheric Physics of the Chinese Academy of Sciences, has constructed the Regional Integrated Environmental Modeling System (RIEMS), which is widely used in studies on East Asian regional climate change and severe weather systems (Scheuch et al., 2015; Xiong et al., 2009). It incorporates atmospheric chemistry and aerosol dynamics into the Regional Integrated Environment Modeling System and produces online simulations of meteorological parameters, aerosol chemical composition, optical characteristics, radiation forcing, and aerosol-induced climate feedback (Li et al., 2014; Li et al., 2013a; Han et al., 2012).

The Nanjing University developed the Regional Climate Chemistry Modeling System (RegCCMS), a synthesis of the regional climate model RegCM2 and the tropospheric atmospheric chemistry model TACM, primarily oriented toward investigating the spatio-temporal distribution, radiation forcing, and climatic effects of tropospheric O_3 and sulfate aerosols (Wang et al., 2004). Subsequently, RegCM3 was coupled with TACM, integrating modules for aerosols into RegCCMS (Wang et al., 2010; Zhang et al., 2014; Li et al., 2009). The system incorporates parameterization schemes facilitating the simulation of aerosols' direct, indirect, and semidirect climatic effects. Extensive evaluations have been carried out regarding major aerosol impacts on the meteorology and regional climate within East Asia (Zhuang et al., 2013; Zhuang et al., 2011; Wang et al., 2015). Subsequently, Shalaby et al. (2012) developed the regional climate-chemistry model RegCM-Chem, by coupling the CBM-Z gas phase chemistry module to version 4 of the RegCM system, RegCM4 (Giorgi et al., 2012). RegCM-Chem also includes a simplified aerosol scheme including radiatively interactive sulfates, carbonaceous aerosols, sea salt, and desert dust (Zakey et al., 2006; Solmon et al., 2006), and it has been used for a variety of applications in different domains.

By developing the regional climate-chemistry-ecology model RegCM-Chem-YIBs, in which the interactive biosphere model YIBs is coupled to RegCM-Chem. The model can produce multi-process simulations of regional climate, atmospheric chemistry, and ecology, especially $PM_{2.5}$, O_3, and CO_2, and their interactions with atmospheric variables (Xu et al., 2023; Ma et al., 2023b; Ma et al., 2023a; Xu et al., 2022; Gao et al., 2022; Xie et al., 2020). Here we expand on these previous studies. We carry out a one-year simulation (2016) at a 30 km horizontal resolution over East Asia with RegCM-Chem-YIBs and conduct a comprehensive assessment. We validate the simulation not only in terms of atmospheric variables but also in terms of atmospheric composition and ecological parameters, by comparison with a range of observations available for this period.

The paper is organized as follows. In section 2 we first describe the RegCM-Chem-YIBs system, focusing

91 in particular on the newly implemented coupling with the ecological component. We also describe the observa-

92 tion datasets used in the model assessment. The simulations are then analyzed in section 3, while section 4 pre-

93 sents our conclusions and a general discussion of our results and future developments.

94 **2 Model and Methods**

95 **2.1 Overall Framework**

96 In RegCM-Chem-YIBs, the atmospheric variables produced by RegCM (temperature, humidity, precipita-

97 tion, radiation, etc.) and atmospheric chemical compounds, such as O_3 and $PM_{2.5}$, produced by the chemis-

98 try/aerosol module are input into YIBs, which simulates the physiological processes of vegetation (such as pho-

99 tosynthesis, respiration, etc.), and calculates land process variables such as CO_2 fluxes, BVOC emissions, and

100 stomatal conductance. The output from YIBs is then fed back to RegCM-Chem, which adjusts the CO_2, O_3, and

101 $PM_{2.5}$ concentrations and their radiative and microphysical effects on the meteorological fields in the lower at-

102 mosphere, thereby achieving a full coupling between climate, chemistry, and ecology. Figure 1 shows the basic

103 framework of the RegCM-Chem-YIBs coupled model.
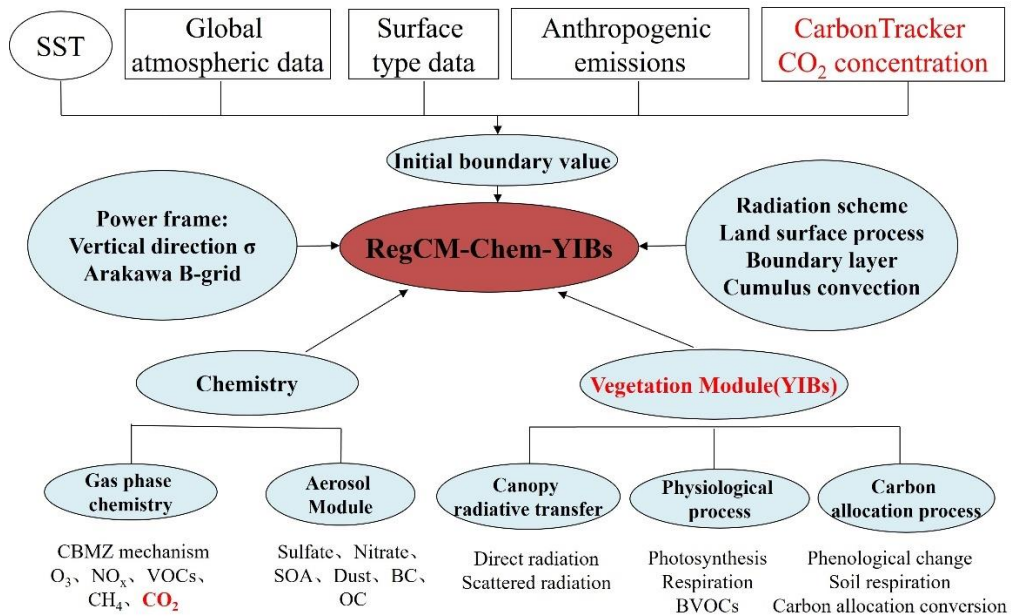
104

105 **Figure 1.** RegCM-Chem-YIBs Coupling Model Framework

106 **2.2 Descriptions of the RegCM-Chem model**

107 The inception of the RegCM system traces back to the late 1980s and early 1990s, when NCAR's (U.S. Na-

tional Center for Atmospheric Research) RegCM 1 was first developed for climate downscaling (Giorgi, 1990; Giorgi and Bates, 1989; Dickinson et al., 1989). After a series of developments, subsequent versions were introduced, such as RegCM2 (Giorgi et al., 1993), RegCM2.5 (Giorgi and Mearns, 1999), RegCM3 (Pal et al., 2007), RegCM4 (Giorgi et al., 2012). The RegCM system presently managed, maintained, and expanded by the Earth System Physics (ESP) section of the Abdus Salam International Center for Theoretical Physics (ICTP), is open-source and extensively employed in regional climate studies, contributing to the establishment of a comprehensive Regional Climate Research Network (RegCNET) (Giorgi et al., 2006). The model can be applied to all regions of the globe (Giorgi et al., 2012) and is moving into a fully-coupled regional Earth system model framework through coupling with the ocean (Turuncoglu et al., 2013; Artale et al., 2010), lake (Small et al., 1999), aerosol (Solmon et al., 2006), dust (Zakey et al., 2006), chemistry (Shalaby et al., 2012), hydrology (Coppola et al., 2003), land surface processes (Oleson et al., 2008). Of specific interest for our study, Shalaby et al. (2012) added a radiatively interactive gas-phase chemical module (CBM-Z) to RegCM4, generating RegCM-Chem, in which atmosphere physics and chemistry are fully coupled.

2.2.1 Aerosol Mechanisms

The RegCM model integrates a simplified aerosol framework, enabling the simulation of sulfate, black carbon (BC), organic carbon (OC), sea salt, and desert dust. The model specifies an external mix of aerosols and accounts for the influence of horizontal advection, turbulent diffusion, vertical transport, emissions, dry and wet deposition, and gas-liquid transition on aerosol concentration (Solmon et al., 2012; Giorgi et al., 2012; Zakey et al., 2006). The secondary organic aerosol scheme VBS (volatile basis set) has also been introduced into the model to further improve RegCM-Chem's simulation of tropospheric aerosols (Yin et al., 2015). The model incorporates the ISORROPIA thermodynamic equilibrium scheme to describe the formation process of secondary inorganic salts, thus enhancing the model's capability to simulate secondary inorganic aerosols (Li et al., 2016b). The further addition of bioaerosols was carried out by Liu (Liu et al., 2016).

2.2.2 Gas phase chemical mechanism

RegCM4-Chem includes the CBM-Z (Carbon Bond Mechanism-Z) atmospheric chemistry mechanism (Zaveri and Peters, 1999). The CBM-IV mechanism, recognized for its widespread use, serves as the basis for CBM-Z (Gery et al., 1989) and was developed to balance simulation accuracy and computational speed. Both

CBM-IV and CBM-Z categorize volatile organic compounds (VOCs) into groups dependent on their carbon bond formation and use lumped species to represent each group. However, CBM-Z includes additional species and reactions compared to CBM-IV, which are crucial for simulating typical urban environments and long-term simulations at regional to global scales. Enhancements in CBM-Z include (1) specific representation of stable alkanes; (2) updated parameters for higher alkanes; (3) separation of olefins into two categories based on differing reactions; (4) addition of peroxy alkane self-reactions significant in low-NOx, such as remote regions; (5) incorporation of reactions among alkanes, peroxyacyl radicals, and NO_3, which are crucial nocturnally; (6) inclusion of long-lived organic nitrates and peroxides; and (7) refinement of isoprene and its peroxy radical chemistry. Collectively, these updates to the CBM-Z chemistry mechanism enhance the model's ability to more accurately simulate long-lived VOCs and address the atmospheric chemistry transition from urban to rural settings.

2.2.3 Radiation scheme

RegCM4 adopts the CCM3 radiation scheme, which uses the delta-Eddington approximation for solar spectral radiation and accounts for the attenuation effect of atmospheric components such as O_3, H_2O, CO_2, O_2 on solar radiation (Kiehl et al., 1998). The CCM3 radiation scheme, implemented in RegCM4, extends from 0.2 to 5 µm, and is segmented into 18 bands. It uses the cloud scattering and absorption parameter scheme, and cloud optical characteristics. As cumulus clouds form, the cloud optical characteristics stretch from the cloud base up to the cloud top, and the radiation calculations assume random overlap. It is assumed in the model that the cloud thickness is equivalent to that of the model's vertical layers, with distinctive cloud water and ice contents assigned to high, middle, and low clouds (Slingo, 1989).

2.2.4 Photolysis rate

Meteorological conditions and chemical input fields determine the photolysis rate, with most variables dynamically produced by the RegCM's modules and updated every 3-30 minutes. SO_2 and NOx, inverted from the US standard atmosphere's vertical profile, are model-defined. Owing to the computational demands of precise photolysis rates from the Tropospheric Ultraviolet–Visible Model (TUV) method (Madronich and Flocke, 1999) and eight data stream spherical harmonics discretization, a look-up table and interpolation method are adopted. Considering the significant impact of clouds on the photolysis rate, it becomes crucial to adjust the cloud amount. Here we use the cloud optical depth information for each grid cell within the model. As the

162 absorption and scattering of ultraviolet radiation by clouds reduce the photolysis rate inside and below the cloud

163 while enhancing it above the cloud, the correction value for the photolysis rate under clear sky conditions de-

164 pends on the position to the cloud layer. Hence, cloud height and optical depth are necessary for the photolysis

165 rate computation (Chang et al., 1987).

2.2.5 Deposition Processes

167 In the model, dry deposition serves as the principal removal process for trace gases, with the deposition

168 velocity being determined by three categories of resistance: aerodynamic, quasi-laminar sublayer, and surface

169 resistance, encompassing soil and vegetation absorption. The latter is inclusive of both stomatal and nonstomatal

170 absorption. The dry deposition module, taken from the CLM4 surface scheme, covers 29 gas-phase species and

171 comprises 11 types of land cover. To enhance the accuracy of the daily variation in dry deposition simulation,

172 both stomatal and nonstomatal resistances are accounted for in the dry deposition scheme. The calculation of all

173 deposition resistances is performed within the CLM land surface model (Wesely, 1989). Wet deposition uses the

174 MOZART global model's wet deposition parameterization scheme (Emmons et al., 2010; Horowitz et al., 2003),

175 including 26 gas-phase species in CBM-Z, and the wet deposition amount is based on the simulated precipita-

176 tion.

2.3 Descriptions of the YIBs model

178 The YIBs model, pioneered by Yale University, integrates plant physiological mechanisms to simulate how

179 photosynthesis, respiration, and other physiological processes respond to environmental drivers such as radia-

180 tion, temperature, and moisture. Moreover, YIBs simulates the carbon cycle both regionally and globally (Yue

181 and Unger, 2015). For example, its simulation of terrestrial carbon flux closely matches ground flux observa-

182 tions and satellite-derived data in diverse geographical areas such as the United States and China (Yue and

183 Unger, 2017; Yue et al., 2017).

2.3.1 The main processes in YIBs

185 In the YIBs model, eight distinct Plant Functional Types (PFTs) are incorporated, encompassing evergreen

186 coniferous forest, evergreen broad-leaved forest, deciduous broad-leaved forest, shrub forest, tundra, C3 grass-

187 land, C4 grasslands, and crops. The model employs the Michaelis–Menten enzyme-kinetics scheme for simulat-

ing plant photosynthesis (Farquhar et al., 1980), and the total photosynthesis (A_{tot}) of leaves is affected by Rubisco enzyme activity (J_c), electron transfer rate (J_e), and photosynthetic product (triose phosphate) transport capacity (J_S) limitation.

2.3.2 Canopy Radiation Scheme

A multilayer canopy radiation transmission scheme is adopted in YIBs for canopy radiation transmission (Spitters et al., 1986), consisting of a radiation transfer model based on the total leaf area index, extinction coefficient, and vegetation height. The entire vegetation canopy is usually divided into 2 to 16 layers, and the specific number of layers can be automatically adjusted according to the height of the canopy.

2.3.3 Biogenic Volatile Organic Compound Emission Scheme

Differently from the traditional MEGAN scheme, the YIBs model applies a biogenic volatile organic compound (BVOC) emission scheme on a leaf scale, which is better suited to describe the photosynthesis process in vegetation (Guenther et al., 1995). This introduces an effect of plant photosynthesis on BVOC emissions which is more closely related to the real physiological process of vegetation. BVOC emissions from leaves to the canopy are integrated to obtain total canopy emissions. The intensity of leaf BVOC emission depends on the rate of photosynthesis J_e under electron transfer rate limitation, leaf surface temperature, and intracellular CO_2 concentration (Yue and Unger, 2015):

$$I = J_e \cdot \beta \cdot \kappa \cdot \tau \cdot \varepsilon , \qquad (1)$$

where I is the intensity of leaf BVOC emission in units of μmol m^{-2}[leaf] s^{-1}. J_e is the electron transport-limited photosynthesis rate, the calculation formula is as follows:

$$J_e = a_{leaf} \cdot PAR \cdot \alpha_{qe} \cdot \frac{C_i - \Gamma^*}{C_i - 2\Gamma^*} , \quad (2)$$

where a_{leaf} is the leaf-specific light absorbance, PAR is photosynthetically active radiation, α_{qe} is the intrinsic quantum efficiency for photosynthetic CO_2 uptake in the chlorophyll reaction system. C_i is the internal leaf CO_2 concentration. Γ^* is the CO_2 concentration compensation point in the absence of non-photorespiratory respiration (Collatz et al., 1991).

β is the coefficient for converting electron transfer flux into BVOC emissions (Niinemets et al., 1999; Pacifico et al., 2011):

$$\beta = \frac{C_i - \Gamma^*}{6(4.67C_i + 9.33\Gamma^*)} , \qquad (3)$$

215   where κ is related to the internal leaf CO_2 concentration:

216 $$\kappa = \frac{C_{i\_standard}}{C_i} , \qquad (4)$$

217   where $C_{i\_standard}$ is the internal leaf CO_2 concentration under standard conditions (when atmospheric CO_2 is

218   370 ppm). The τ term reflects the response of BVOC emission intensity to temperature:

219 $$\tau = \exp[0.1(T - T_{ref})] . \qquad (5)$$

220   where T is the blade surface temperature, T_{ref} is the standard temperature (30 °C). When the blade temperature

221   is 40 °C, the BVOC emission intensity is maximum. As the temperature further rises, the BVOC emission grad-

222   ually weakens. In reality, such high temperatures are relatively rare and may only occur under extremely dry

223   climate conditions.

224   **2.3.4 Ozone Damage Protocol**

225   When tropospheric ozone enters plants through stomata, it can directly damage plant cell tissues, thereby

226   slowing the photosynthesis rate and further weakening the carbon sequestration capacity of vegetation. The

227   YIBs model incorporates the semi-mechanistic parameterization scheme to delineate ozone's effect on plants

228   (Sitch et al., 2007):

229 $$A = A_{tot} \cdot F , \qquad (6)$$

230   where A is photosynthesis minus the influence of ozone, A_{tot} is the total photosynthesis of leaves, F is the

231   proportion of photosynthesis minus the influence of ozone, which depends on the ozone flux from the stomata

232   into the vegetation that exceeds the threshold.

233 $$F = 1 - a \cdot \max[(F_{ozn} - F_{ozncrit}), 0] , \qquad (7)$$

234   where a is the sensitivity parameter of vegetation to ozone obtained based on observation data. $F_{ozncrit}$ repre-

235   sents the threshold corresponding to the damage caused by ozone to vegetation, F_{ozn} represents the flux of

236   ozone entering the page through the stomata:

237 $$F_{ozn} = \frac{[O_3]}{r_b + \frac{\kappa_{O3}}{r_s}} , \qquad (8)$$

238   where $[O_3]$ is the ozone concentration at the top of the canopy, r_b is the boundary layer resistance, κ_{O3} is the

239   ratio of O_3 leaf resistance to water vapor blade resistance, r_s is the stomatal resistance considering the influence

240   of ozone:

241 $$r_s = g_s \cdot F . \qquad (9)$$

242   g_s is the leaf conductance without O_3 effects. The set of equations (7), (8) and (9) yields a quadratic term in F

243   that can be solved analytically.

2.4 Descriptions of the RegCM-Chem-YIBs model

2.4.1 Coupling between RegCM-Chem and YIBs

246   The integrated RegCM-Chem-YIBs model, an enhancement to the original RegCM-Chem, introduces CO_2

247   as an atmospheric constituent, incorporating its source-sink dynamics, transport, and diffusion processes. At-

248   mospheric CO_2 concentration is primarily influenced by atmosphere-ocean CO_2 exchange flux, biomass com-

249   bustion emissions, fossil fuel emissions, and terrestrial ecosystem CO_2 flux. The model prescribes fossil fuel

250   emissions, biomass combustion emissions, and atmosphere-ocean CO_2 fluxes, while the terrestrial ecosystem

251   CO_2 fluxes are computed in real time via the coupled YIBs terrestrial ecosystem model.

252   Within the coupled model system, meteorological variables (including temperature, humidity, precipitation,

253   radiation, etc.) and atmospheric pollutant concentrations (O_3 and $PM_{2.5}$) generated by RegCM-Chem are incor-

254   porated into the YIBs model every six-minute intervals. This integration step is to be consistent with the integra-

255   tion time step of the chemistry module, thus maintaining synchronization between modules. Considering the

256   complexity of chemical reactions and ecological processes, dynamic adjustments at short intervals enable the

257   model to better capture transient interactions between ecology and the atmosphere. The choice of this adjust-

258   ment frequency balances the representation of actual processes with computational efficiency, ensuring that

259   simulation results are both accurate and efficient. YIBs then simulates vegetation physiological processes such

260   as photosynthesis and respiration, computing land surface parameters including CO_2 flux, BVOC, and stomatal

261   conductance. These outputs from the YIBs are subsequently integrated back into the RegCM-Chem model every

262   six-minute intervals, the intricacies of this integration process lead to significant changes in various environ-

263   mental parameters. The major direct changes, prominently influencing the model's behavior, arise from altera-

264   tions in CO_2 concentration. These changes are directly attributed to intricate physiological processes within the

265   vegetation, including photosynthesis and respiration. The fluxes of CO_2 through these biological processes play

266   a pivotal role in shaping the atmospheric composition. On the indirect front, the integration of YIBs outputs in-

267   duces intricate variations in $PM_{2.5}$ and O_3 concentrations. These indirect changes are primarily orchestrated by

268   shifts in BVOC emissions. The dynamic nature of these emissions contributes to the complexity of atmospheric

269   chemistry, influencing the levels of $PM_{2.5}$ and O_3. Simultaneously, the integration process plays a crucial role in

270 shaping the temporal variations of atmospheric temperature, humidity, and circulation. These changes over time

271 are intricately linked to variations in land surface parameters. The interplay of these variables illustrates the dy-

272 namic feedback loops between climate, chemical composition, and ecological processes within the integrated

273 model system.

2.4.2 Model input data

275 The input data of RegCM-Chem-YIBs mainly includes four categories: surface data, initial boundary data,

276 anthropogenic emission data and CO_2 surface flux data, which are detailed below.

277 (1) Surface data include surface vegetation cover type, terrain, and leaf area index. Land cover type infor-

278 mation is obtained from the MODIS and AVHRR satellites, employing the classification scheme suggested by

279 Lawrence and Chase (Lawrence and Chase, 2007), which uses MODIS data to preliminarily distinguish forest,

280 grassland, bare soil, etc., and combine this with AVHRR data to make a detailed forest classification. The dataset

281 contains a total of 16 different vegetation functional types. To align with the classification conventions of the

282 YIBs model, the original 16 vegetation functional types were converted into the corresponding 8 types recog-

283 nized by the YIBs model. The results are shown in Figure S1.

284 (2) Initial and boundary data include initial and boundary conditions of meteorological variables and at-

285 mospheric chemical composition. Here we use ERA-Interim reanalysis meteorological data, a product from the

286 European Center for Medium-Range Weather Forecasts (ECMWF) created through four-dimensional variational

287 assimilation. The data is on 37 vertical levels, with a horizontal resolution of 0.125°×0.125°, and time resolution

288 of 6 hours. Data for Sea Surface Temperature (SST) is provided by the weekly averaged Optimum Interpolation

289 SST product (OI_WK) of the National Oceanic and Atmospheric Administration (NOAA) (Reynolds et al.,

290 2002). The initial and boundary conditions of atmospheric chemical components (e.g. O_3), come from simula-

291 tions carried out with the global chemistry model MOZART (Emmons et al., 2010; Horowitz et al., 2003). In

292 addition, the initial and boundary conditions for CO_2 species come from the CarbonTracker global carbon as-

293 similation system (Peters et al., 2007) developed by NOAA Earth System Research Laboratory ESRL (Earth

294 System Research Laboratory), which uses the ensemble Kalman filter algorithm to assimilate ESRL greenhouse

295 gas observations and CO_2 observation data provided by the network of collaborating institutions worldwide. The

296 assimilated data includes not only conventional fixed-site observations but also mobile monitoring data such as

297 aircraft and ships. Since 2007, yearly updated carbon assimilation products are provided by CarbonTracker, de-

298   livering global CO_2 three-dimensional concentration data products every three hours. In this study, we utilized

299   the CT2019 product, updated in 2019, spanning a period from January 1, 2000 to March 29, 2019.

300   (3) Anthropogenic emission data include precursors of ozone and particulate matter such as NOx, VOC,

301   BC, OC, etc. The MIX Asian anthropogenic emission inventory developed by the Tsinghua University is used

302   (Li et al., 2017b), which integrates the results of the emission inventories of various regions in Asia. The emis-

303   sions in China come from China's multi-scale emission inventory MEIC (Multi-resolution Emission Inventory

304   for China) and the high-resolution NH_3 emission inventory developed by Peking University. The anthropogenic

305   emissions in India come from the Indian local emission inventory developed by ANL (Argonne National Labor-

306   atory), while the anthropogenic emissions in South Korea come from the CAPSS (The Korean local emission

307   inventory developed by the Policy Support System), and the man-made emissions in other regions are provided

308   by the REAS (Regional Emission inventory in Asia) emission inventory version 2.1. The anthropogenic emis-

309   sions of major pollutants in the simulated area are shown in Figure S2.

310   (4) Data pertaining to fossil fuel CO_2 emissions are sourced from the MIX Asian anthropogenic emission

311   inventory with a monthly time resolution. CO_2 emissions resulting from biomass burning are derived from the

312   FINN (Fire Inventory from NCAR) inventory (Wiedinmyer et al., 2011) developed by the National Center for

313   Atmospheric Research. The FINN inventory has a daily time resolution. The model's ocean-atmosphere CO_2

314   exchange flux is obtained from the carbon flux product of the CarbonTracker assimilation system, constructed

315   with the global atmospheric transport model TM5 and assimilating CO_2 observation data via an ensemble Kal-

316   man filter algorithm. This provides global $1° \times 1°$ resolution CO_2 exchange flux data between the ocean and the

317   atmosphere updated every three hours. The emissions are detailed in Figure S3.

318   **3 Model Application**

319   **3.1 Model setup**

320   To evaluate the performance of RegCM-Chem-YIBs we carried out a one-year simulation starting from

321   December 1st, 2015, through December 31st, 2016. The initial month is used as spin-up period, and thus it is not

322   included in the analysis. The simulation domain is centered at 36°N, 107°E, and covers a considerable part of

323   East Asia, including China, Japan, the Korean Peninsula, and Mongolia, along with significant parts of India and

324   Southeast Asia (Figure S4). The horizontal grid spacing is 30 km and we use 14 levels in the vertical, reaching

325 up to 50 hPa. Section 2.4.2 provides a comprehensive description of the model input data.

3.2 Climate simulations in East Asian

327   Given the importance of the climate for the East Asia region, we first present an assessment of the simula-

328 tion for the climate 2016 by comparison with the ERA-Interim data. The simulated temperature, specific

329 humidity, and wind fields at varying altitudes and seasons compared well with the reanalyzed data (Figure S5~

330 Figure S9), especially temperature and specific humidity, while a tendency to overestimate wind speed is

331 observed at the near surface and 850 hPa levels. The fields at 500 hPa show very close agreement with

332 reanalysis data, indicating a strong mid-atmosphere forcing by the boundary conditions, while the simulated

333 circulation patterns near the surface and at 850 hPa in summer tend to deviate more from the driving reanalysis.

334 The simulated circulation patterns in the other seasons are basically consistent with the reanalysis data.

335   We first calculated the daily average of the meteorological variables, such as temperature, wind speed, and

336 specific humidity, from the model simulation and reanalysis data, respectively. Then we calculate the

337 corresponding statistical indicator correlation coefficient (R), mean deviation (MB), and root mean square error

338 (RMSE) based on the daily averages. Table 1 reports a number of statistical metrics of comparison between

339 simulated and reanalysis meteorological variables at different heights. Correlation coefficients (R) range from

340 0.95 to 0.98 for temperature, 0.71 to 0.97 for longitudinal wind, 0.81 to 0.92 for latitudinal wind, and 0.91-0.92

341 for specific humidity, indicating a general good consistency between model and driving data, in line with previ-

342 ous studies (Zhuang et al., 2018; Zhou et al., 2014; Wang et al., 2010).

343 **Table 1.** Statistical indicators for comparison between model simulation results and reanalysis data

Heights	Statistical index	Air Temperature(K)	Longitudinal wind (m/s)	Latitudinal wind (m/s)	Specific humidity (kg kg^{-1})
	R	0.98	0.97	0.92	0.91
500 hpa	MB	0.15	0.35	-0.03	0.00015
	RMSE	0.93	0.75	0.51	0.00019
	R	0.96	0.77	0.85	0.94
850 hpa	MB	-0.98	0.38	0.15	-0.00066
	RMSE	1.1	1.08	0.59	0.00077
Near sur-	R	0.95	0.71	0.81	0.92

face	MB	-1.21	0.33	0.23	-0.00098
	RMSE	1.35	0.59	0.54	0.00112

(Correlation coefficients (R), mean biases (MB), and root mean square error (RMSE))

The magnitude of surface radiation flux directly determines the rates of photosynthesis in vegetation. For verification purposes, model surface solar fluxes were compared with data on solar energy at the surface retrieved from the Clouds and the Earth's Radiant Energy System (CERES) satellite, which has a $1° \times 1°$ horizontal and monthly temporal resolution. Figure S10 shows the simulated surface net shortwave radiation in different seasons and comparison with observational data. The model tends to overestimate surface net shortwave radiation in spring and winter over India and summer over North China (Yin et al., 2014). Overall, the simulated surface net shortwave radiation agrees well with the CERES satellite retrieval results, capturing the spatial distribution and seasonal fluctuation patterns of surface shortwave radiation. The simulation findings from our study are consistent with earlier research regarding surface net shortwave radiation (Han et al., 2016).

In conclusion, RegCM-Chem-YIBs demonstrates a good performance in simulating the climatological features of the East Asia atmospheric circulations, effectively reproducing the spatial distribution and seasonal variations of temperature, specific humidity, and radiation.

3.3 Simulations of $PM_{2.5}$**,** O_3 **and** CO_2

In this section, we compare simulated $PM_{2.5}$ and O_3 concentrations against observational data from 366 stations provided by the China National Environmental Monitoring Center. The geographical distribution of the simulated annual mean near-surface daily $PM_{2.5}$ and maximum daily 8-hour average (MDA8) O_3 concentration, along with the observed values, are shown in Figure 2. Supplementary Figure S11 then compares in a scatter-plot format the observation and simulation results. Both figures demonstrate that the model reproduces the spatial distribution patterns of $PM_{2.5}$ and O_3, with a significant agreement between modeled and measured values across all stations. The statistical indicators of simulated and measured surface $PM_{2.5}$ and O_3 levels are shown in Table S1, showing a correlation between simulation and observations of O_3 and $PM_{2.5}$ of 0.74 and 0.65, respectively. The simulated O_3 concentrations are generally lower than observed in the Fenwei Plain of China, a discrepancy possibly attributable to uncertainties in the emission inventory for this region. In summary, the RegCM-Chem-YIBs model demonstrates a good ability to capture the spatial distribution of observed near-surface ozone and particulate matter, especially in highly polluted areas.
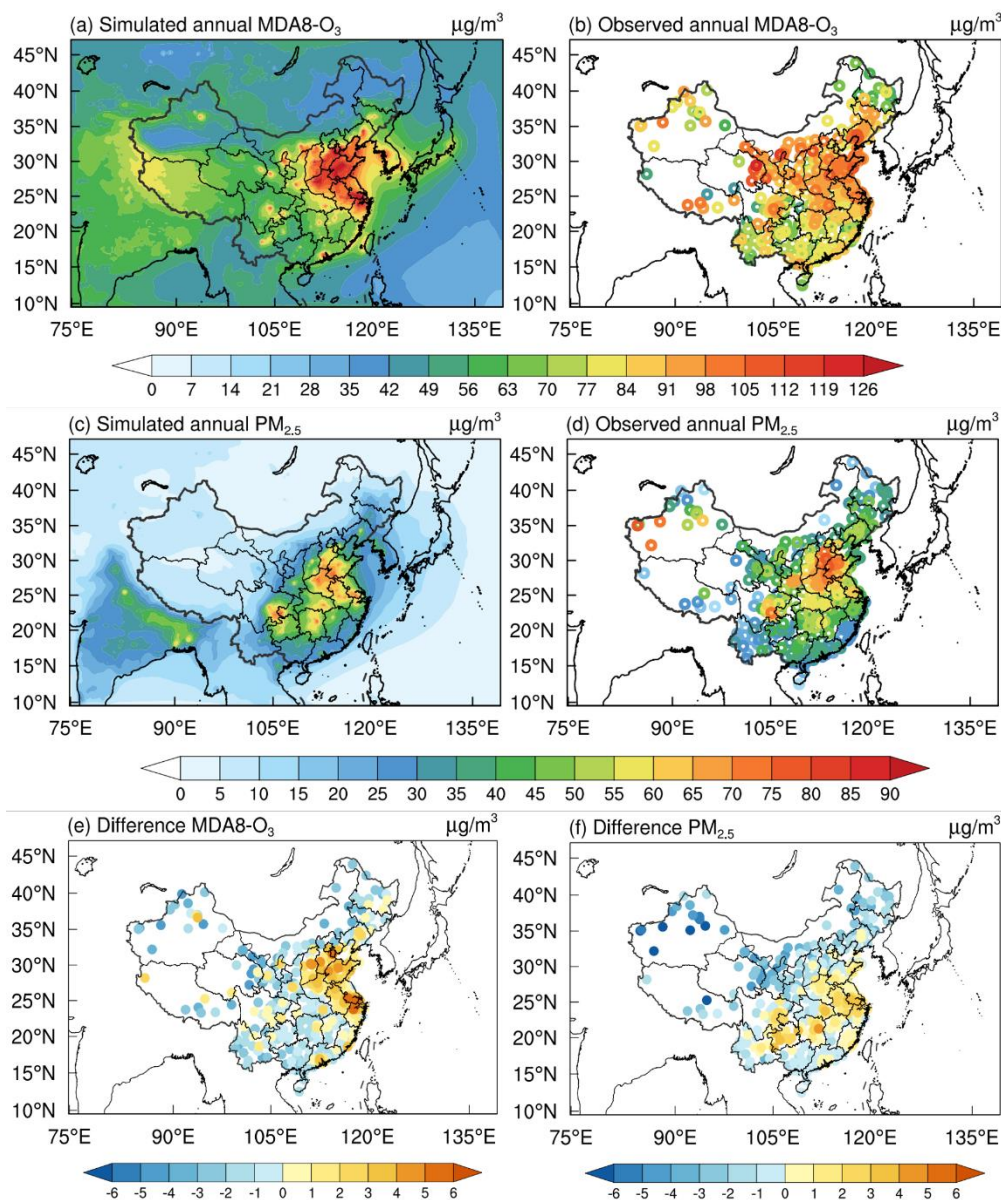
Figure 2. Simulation and observation comparison of (a, b) O_3 and (c, d) $PM_{2.5}$ and their differences (e, f) in China. The differences are simulation minus observation. The colored circles in the figure represent station observations. Units: $\mu g\ m^{-3}$.

Measured and calculated monthly mean CO_2 concentrations at six observation stations in East Asia from the World data Center for Greenhouse Gases are shown in Figure 3. Information on the six sites is listed in Table 2. The simulated CO_2 concentration agrees well with observations, with correlation coefficients ranging from 0.89 to 0.97. However, in urban and coastal areas, the model performance deteriorates likely due to local emission fluctuations and errors in biogenic fluxes. Nevertheless, the model overall captures the seasonal variations in CO_2 concentrations (Figure 3). This result likely stems from the complex relationship between biogenic and fossil fuel emissions, which are known contributors to observed seasonal CO_2 patterns (Kou et al., 2015). A high

381 CO_2 mixing ratio (412.3 ppm) is observed at the TAP site, which is associated with strong local emissions. Fur-
382 ther analysis into the specific sources contributing to elevated CO_2 levels would provide valuable insights into
383 localized patterns of emissions and their effects on regional carbon cycle processes. The model's ability to re-
384 produce the geographical and seasonal CO_2 patterns serves as an illustration of its ability to capture the main
385 processes driving CO_2 dynamics. In summary, while discrepancies in urban or coastal areas highlight the chal-
386 lenges associated with capturing localized CO_2 dynamics, the model's overall performance and ability to repro-
387 duce geographical and seasonal CO_2 patterns demonstrates its usefulness in studying CO_2 dynamics at a regional
388 scale.

389 **Table 2.** Information on six CO_2 stations in East Asia and statistical indicators of observed and modeled CO_2.

Sites	Latitude	Longitude	Elevation	Observations (ppm)	Simulations (ppm)	R	RMSE
WLG	36.29	100.90	3810	404.3	402.9	0.94	1.75
TAP	36.72	126.12	20	412.3	414.8	0.97	2.70
UUM	44.45	111.08	992	405.7	403.7	0.96	2.66
LLN	23.46	120.86	2867	406.0	407.2	0.93	1.63
YON	24.47	123.02	30	407.1	407.4	0.89	2.80
HK	22.31	114.17	65	407.9	409.7	0.92	15.67

390 (Correlation coefficients (R) and root mean square error (RMSE))

391
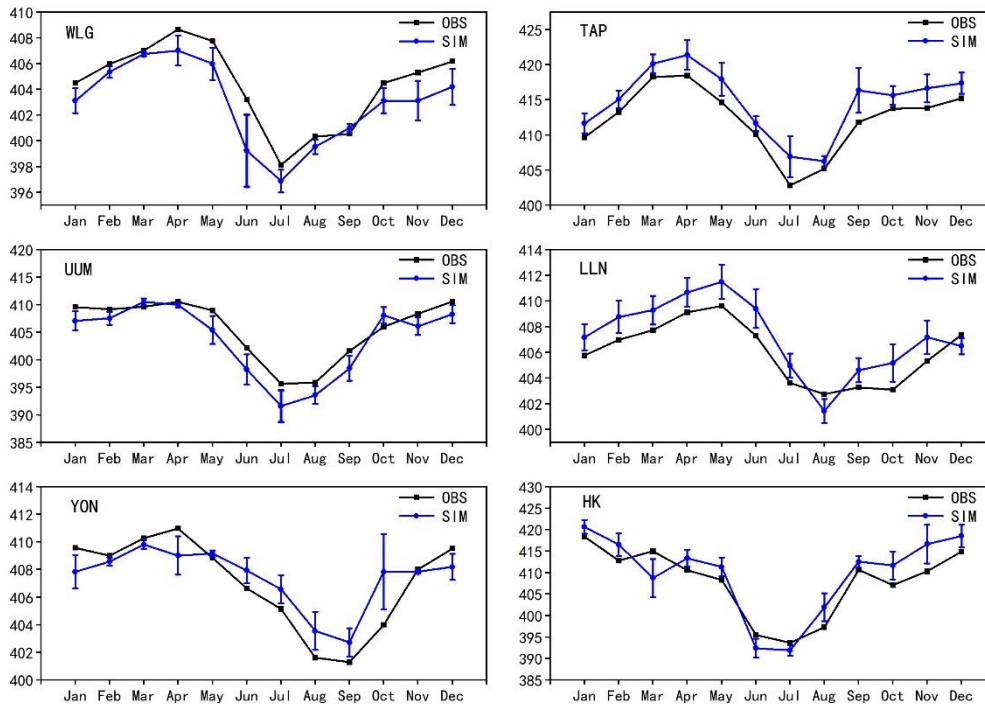
Figure 3. Modeled (blue) and observed (black) monthly mean CO_2 concentrations validated at six sites in East

Asia. Units: ppm.

The limitations of ground-based CO_2 observation stations, particularly their sparse spatial distribution, pose

challenges in obtaining high-resolution CO_2 data. To offset this limitation, data assimilation methods have been

implemented to ensure a coherent global distribution of atmospheric CO_2, effectively filling the void left by

sparse ground-based observations. Here we utilize the Carbon Tracker global carbon assimilation system

developed by the NOAA Earth System Research Laboratory (ESRL) to validate the simulated CO_2

concentrations (Peters et al., 2007). This comparison for the year 2016 is shown in Figure 4. The simulated CO_2

concentrations tend to be lower than observed in Northeastern India and Northeastern China, while they show a

better agreement with observations in other regions. These discrepancies can be traced back to factors such as

the underestimation of localized CO_2 emissions along with the effects of complex topography and circulation

patterns. However, the closer agreement in other regions suggests that the model effectively captures the

primary processes driving CO_2 concentrations.

Seasonal variations in the spatial distribution of CO_2 concentrations for 2016 are illustrated in supplemen-

tary Figure S12. The simulations show marked seasonal variations, with elevated concentrations in spring,

autumn, and lower values during summer. In northern regions, including Russia, Mongolia, and Northeast China,

the lowest near-surface CO_2 concentrations occur in summer. This pattern can be attributed to the enhanced

photosynthetic activity of terrestrial vegetation in summer, leading to enhanced atmospheric CO_2 sequestration. Conversely, winter months are characterized by lower solar radiation fluxes and reduced vegetation photosynthesis, resulting in relatively higher CO_2 concentrations. In specific regions, notably the eastern coastal zones of China and South Korea, the seasonal pattern of CO_2 concentration is reduced, likely because of the high levels of urbanization, dense population, and intense anthropogenic emissions in these areas. In contrast, regions such as Yunnan, the southern side of the Qinghai-Tibet Plateau, and Southeast Asia exhibit consistently low CO_2 concentrations during summer because of significant vegetation sinks in these densely vegetated areas. An increase in CO_2 concentrations can be observed over these regions during spring due to local forest fires and straw-burning processes, which release substantial amounts of CO_2 into the atmosphere (Chuang et al., 2014).
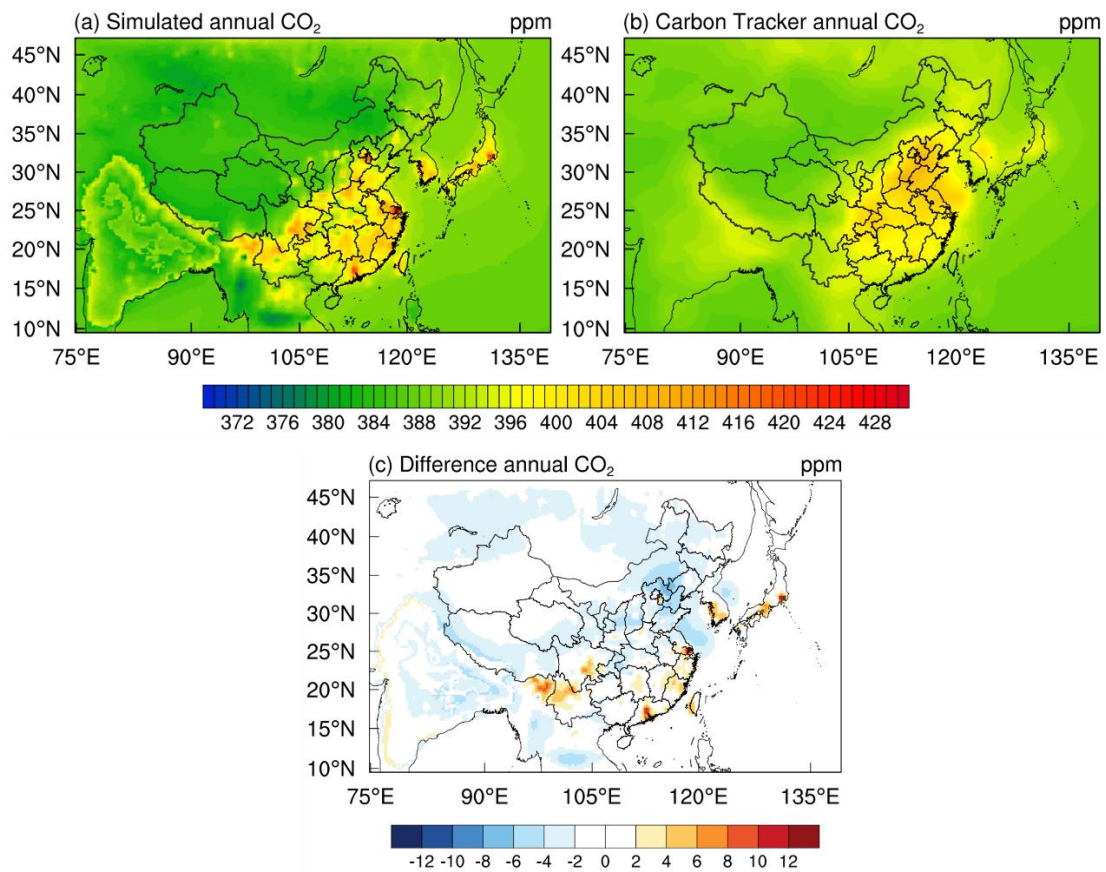
Figure 4. Evaluation of simulated CO_2 (a) using Carbon Tracker products (b) and their difference (c) in 2016. The differences are simulation minus observation. Units: ppm.

3.4 Simulations of carbon fluxes in terrestrial systems

Our assessment of GPP and NPP uses the MOD17A3 Collection 6, a global product originating from MODIS satellite observations. GPP data include 8-day values with a resolution of 500 meters, as produced in

424 MOD17A2H Version 6 based on radiation use efficiency theory. Such data can be used as input to computations

425 of terrestrial carbon and energy flows, water cycling processes, and vegetation biogeochemistry. Moreover, the

426 MOD17A3H Version 6 product provides information on annual NPP, also on a resolution of 500 meters. All

427 8-day Net Photosynthesis (PSN) products (MOD17A2H) from a particular year are combined to derive annual

428 NPP values (He et al., 2018; Madani et al., 2014; Running, 2012).

429 Figure 5 (a, b, e) shows the geographical distribution of the mean GPP in 2016 from the model simulations

430 and MODIS products. RegCM-Chem-YIBs effectively captures the observed spatial GPP features, with high

431 values mostly over Southwest, Central, and Southeastern China, areas characterized by deciduous broad-leaf

432 and evergreen coniferous forests (Figure S1). The annual average GPP simulated by RegCM-Chem-YIBs is

433 higher than observed over   Southwest and Central China by 6.8% and 12.7%, respectively. The annual average

434 simulated GPP over China is 6.18 Pg C yr^{-1}, which is about 7.56% higher than the GPP in MODIS.

435 Figure 6 (a) and Table S2 show the scatter plots of the simulated annual average GPP on each model grid

436 point compared with MODIS. A correlation coefficient of 0.91 and root mean square error of 0.4 kg C m^{-2} yr^{-1} is

437 found,   reflecting an overall good simulation by the model. Compared with the results obtained from the global

438 model NASA ModelE2–YIBs (Yue and Unger, 2017), the GPP value estimated here compares better with the

439 MODIS product, which may also be attributed to the higher spatial resolution of the regional system. Moreover,

440 our GPP results are also in line with earlier findings, such as from Li (Li et al., 2013b) who estimated an annual

441 average GPP over China of 6.04 Pg C yr^{-1} based on the light energy utilization model EC-LUE.

442 Figure 5 (c, d, f) shows the spatial distribution of mean NPP for both the simulations and MODIS

443 products in 2016. NPP, similarly to GPP, exhibits a gradual reduction from southeast to northwest China. The

444 scatter plot comparing the simulated and MODIS annual average NPP across the model grid is illustrated in

445 Figure 6 (b). According to Table S2, a correlation coefficient of 0.87 is found between the simulated and

446 MODIS NPP, with a root mean square error of 0.22 kg C m^{-2} yr^{-1}. Notably, the simulated NPP shows a distinct

447 underestimation over regions with higher NPP values. Compared with the MODIS NPP data products, the

448 annual average NPP simulated for the entire China region in 2016 is overestimated by approximately 8.64%,

449 mostly because of the model overestimate in Central China (16.6%).

450 Part of the reason for this result is the relatively simple treatment of the nitrogen deposition process in YIBs

451 (Yue and Unger, 2015). On the other hand, some studies have noted that due to the limitations of driving data

452 and algorithm parameters, the MODIS NPP products have some problems in China (Li et al., 2013b).

453 Furthermore, the NPP value estimated by the model over China is 3.21 Pg C yr^{-1}, in line with the mean value

454 (2.92 ± 0.12 Pg C yr^{-1}) found in previous 37 studies (Wang et al., 2017).
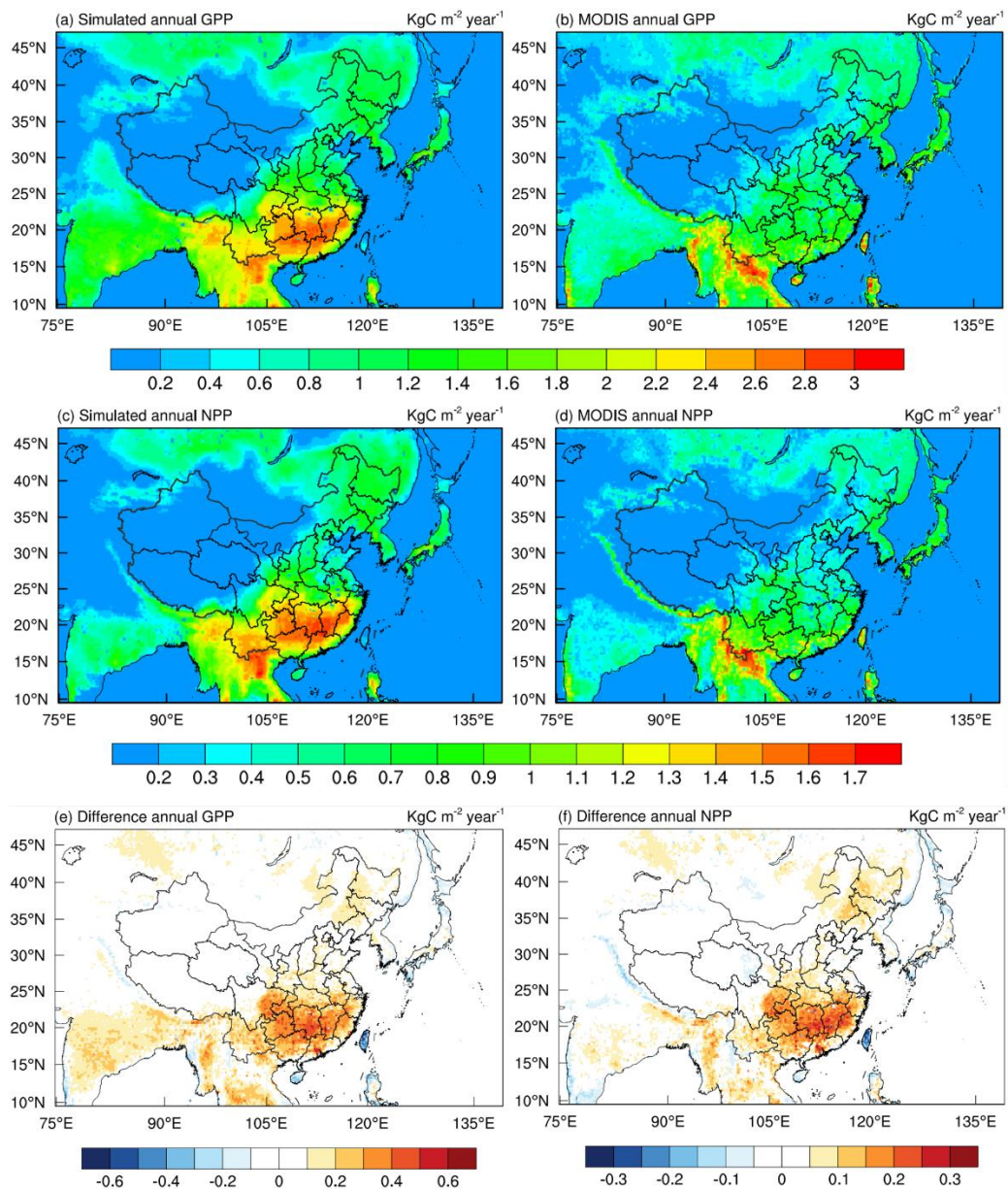
455

456 **Figure 5.** Spatial distribution of modeled (a, c) and MODIS (b, d), annual mean GPP (a, b) and NPP (c, d), and

457 their differences (e, f). The differences are simulation minus observation. Units: kg C m^{-2} year^{-1}.
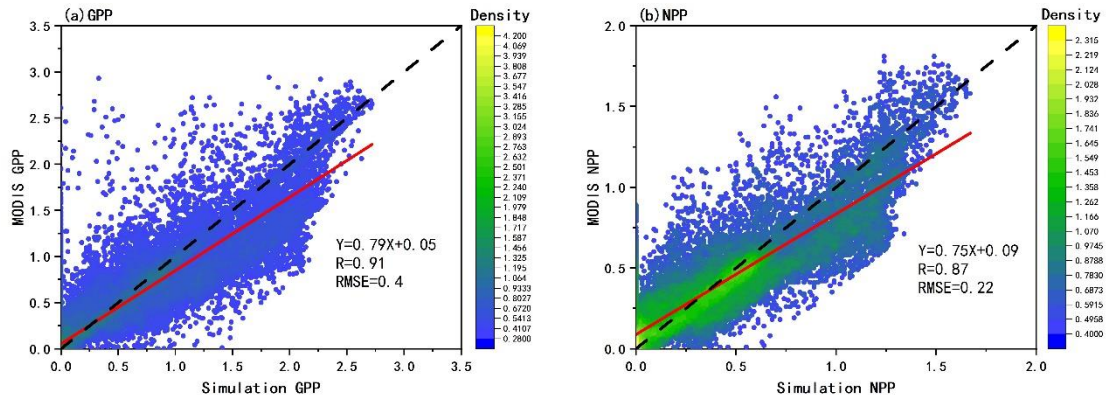
458

459 **Figure 6.** Density scatter plots of (a) GPP and (b) NPP for model simulations and inversion-based products for

460 2016. Units: kg C m^{-2} year^{-1}.

461   Figure 7 and Figure 8 illustrate the seasonal fluctuations in GPP and NPP, as simulated for 2016 in East

462 Asia. Both GPP and NPP present pronounced seasonal variations, with negligible values during winter, and a

463 strong peak in summer.   The winter minimum is attributable to limiting environmental factors such as reduced

464 solar radiation, lower temperatures, and suppressed photosynthetic activity by vegetation. Conversely, summer

465 shows the highest GPP and NPP values due to extended daylight hours, increased solar radiation, and

466 temperatures facilitating increased photosynthetic activity and vegetation metabolism.
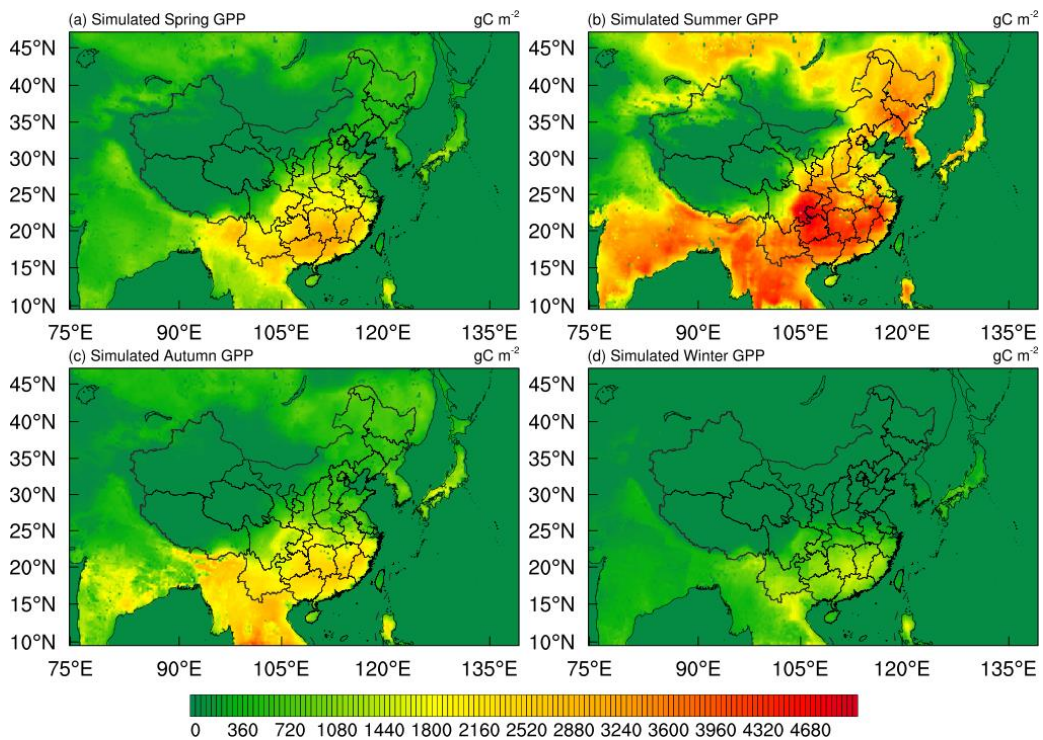
467

468 **Figure 7.** Spatial distribution of GPP simulated by model of spring(a), summer(b), autumn(c) and winter(d) in

469 2016. Units: g C m^{-2}
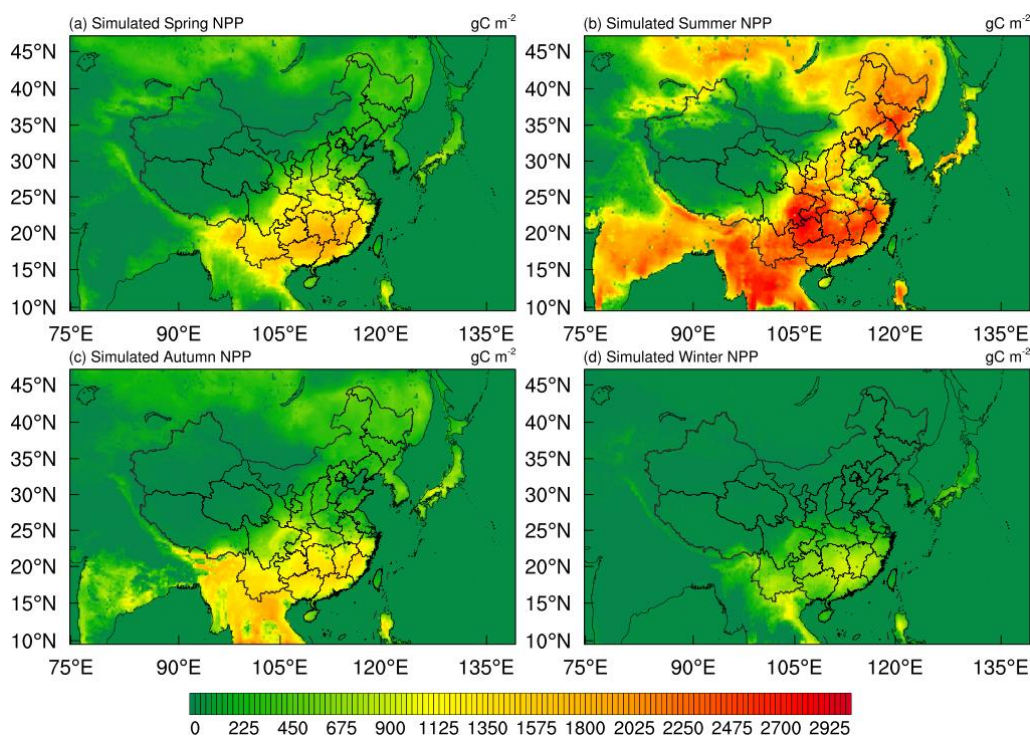
Figure 8. Spatial distribution of NPP simulated by model of spring(a), summer(b), autumn(c) and winter(d) in 2016. Units: g C m^{-2}

3.5 Simulations of other carbon-bearing species

The analysis of additional carbonaceous compounds such as BC, OC and carbon monoxide (CO), is crucial due to their considerable influence on climate and the carbon cycle. The spatial distribution of simulated BC for each season of 2016 is shown in Figure S13. BC concentrations are mainly centered in North China, Central China, the Sichuan Basin, Chongqing, and Northeast India, regions with a higher concentration of industrial and residential emission sources. BC displays a marked seasonal variation, with elevated levels in winter, possibly attributed to residential heating, more stagnant conditions, and reduced removal by precipitation.

Figure S14 then shows the spatial corresponding distribution of seasonal OC, which is also higher over North China, Central China, Sichuan and Chongqing, and Northeast India. Finally, Figure S15 reports the annual mean near-surface CO concentrations for observations and simulation data across the monitoring sites in China. While simulated CO concentrations agree well spatially with observations, the simulations produce higher values than observed in Central China, likely linked to uncertainties in emission inventories. Figure S16 presents the seasonal spatial distributions of CO, with simulated high values mostly localized in Sichuan-Chongqing and Central China, and a peak in winter.

4 Conclusions

Regional climate-chemical coupled models can be used to study the characteristics of regional-scale climate and pollutants, and is an important means to investigate the behavior of atmospheric pollutants and their radiative climate effects. However, current coupled regional climate models describe the physiological process of terrestrial vegetation relatively simply and do not consider the interaction between atmospheric pollutants (such as $PM_{2.5}$ and O_3) and CO_2, as well as their impacts on terrestrial ecosystems.

To overcome this problem, in this work we coupled the YIBs biogeochemical model to the RegCM-CHEM regional climate-chemistry model, and tested this coupled modeling system over a domain covering East Asia at a 30 km horizontal grid spacing for the year 2016. The model output was validated against reanalysis data, observational data, and satellite remote sensing data, both for the atmosphere and the carbon cycle.

Our simulations show that the coupled RegCM-Chem-YIBs system can effectively reproduce the spatio-temporal distribution of meteorological variables, atmospheric composition ($PM_{2.5}$, O_3, and CO_2) and terrestrial carbon fluxes (GPP and NPP). Comparisons of the simulated temperature, longitudinal wind, latitudinal wind, and specific humidity for different seasons with the driving ERA-Interim reanalysis data showed correlation coefficients of 0.95-0.98, 0.71-0.97, 0.81-0.92, and 0.91-0.92, respectively. The correlation coefficients between observed and simulated O_3 and $PM_{2.5}$ levels in China were 0.74 and 0.65, respectively, while the corresponding correlations for CO_2 were in the range of 0.89 to 0.97. Comparison of the ecological parameters GPP and NPP simulated in East Asia with the observed data showed correlation coefficients of 0.91 and 0.87, respectively. In addition, in all cases, the seasonal variation of the different variables was captured by the model. Therefore, we conclude that, overall, the RegCM-Chem-YIBs model demonstrates a good performance in simulating the spatio-temporal distribution characteristics of regional meteorological characteristics, atmospheric composition, and ecological parameters over East Asia.

In the future, we will continue to improve RegCM-Chem-YIBs in the following aspects. First, we will investigate the impact of CO_2 and O_3 inhomogeneity on radiation calculations by integrating temporally and spatially varying concentrations derived from YIBs and Chem into the RegCM radiation module. This will enable additional accurate computation of longwave radiation flux, improving the representation of the regional radiation balance. Second, we intend to assimilate a module representing various chemical transformations happening on the surfaces of aerosol particles. Finally, we will include the wet removal process of O_3. These advancements will contribute to the refinement of RegCM-Chem-YIBs, enhancing our ability to investigate the interactions

516   between regional atmosphere, carbon cycle, and vegetation processes.

517   **Code and data availability**

518   The RegCM-Chem source code can be obtained from https://github.com/ICTP/RegCM (last access: 10 July

519   2023). The YIBs model code is available at https://github.com/YIBS01/YIBs_site (last access: 10 July 2023).

520   The input data and source code for RegCM-Chem-YIBs have been archived on Zenodo at

521   https://doi.org/10.5281/zenodo.8186164 (Xie et al., 2023). The CarbonTracker data are provided at

522   http://dx.doi.org/10.25925/20201008 (Jacobson et al., 2020). The CERES surface radiation data are available at

523   https://doi.org/10.5067/TERRA+AQUA/CERES/SYN1DEGMONTH_L3.004A (NASA/LARC/SD/ASDC,

524   2017). WDCGG data are available at https://doi.org/10.15138/wkgj-f215 (Lan, 2023). CNEMC data are pro-

525   vided at https://doi.org/10.5281/zenodo.10792015 (Xie, 2024). MODIS data are available at

526   https://doi.org/10.5067/MODIS/MOD17A2H.006 (Running et al, 2015).

527   **Author contributions**

528   TW led the development of RegCM-Chem-YIBs with significant contributions from NX and XX. NX per-

529   formed the evaluation. NX, TW drafted the manuscript and all authors contributed to review and editing of the

530   manuscript.

531   **Competing interests**

532   The corresponding author has stated that all the authors have no conflicts of interest.

533   **Disclaimer**

534   Publisher's note: Copernicus Publications remains neutral about jurisdictional claims in published maps and

535   institutional affiliations.

536   **Acknowledgments**

537   This work was supported by the National Natural Science Foundation of China (42077192), the National Key

538   Basic Research & Development Program of China (2020YFA0607802), the Creative talent exchange program

539   for foreign experts in the Belt and Road countries, and the Emory University-Nanjing University Collaborative

540   Research Grant.

541   **References**

542   Ahlstrom, A., Raupach, M. R., Schurgers, G., Smith, B., Arneth, A., Jung, M., Reichstein, M., Canadell, J. G.*, et*
543   *al.*: The dominant role of semi-arid ecosystems in the trend and variability of the land CO_2 sink, Science,
544   348, 895-899, https://doi.org/10.1126/science.aaa1668, 2015.

545   Ainsworth, E. A., Yendrek, C. R., Sitch, S., Collins, W. J., and Emberson, L. D.: The Effects of Tropospheric
546   Ozone on Net Primary Productivity and Implications for Climate Change, Annu. Rev. Plant Biol., 63,
547   637-661, https://doi.org/10.1146/annurev-arplant-042110-103829, 2012.

548   Artale, V., Calmanti, S., Carillo, A., Dell'Aquila, A., Herrmann, M., Pisacane, G., Ruti, P. M., Sannino, G.*, et al.*:
549   An atmosphere-ocean regional climate model for the Mediterranean area: assessment of a present climate
550   simulation, Clim. Dyn., 35, 721-740, https://doi.org/10.1007/s00382-009-0691-8, 2010.

551   Baklanov, A., Molina, L. T., and Gauss, M.: Megacities, air quality and climate, Atmos. Environ., 126, 235-249,
552   https://doi.org/10.1016/j.atmosenv.2015.11.059, 2016.

553   Chang, J. S., Brost, R. A., Isaksen, I. S. A., Madronich, S., Middleton, P., Stockwell, W. R., and Walcek, C. J.: A
554   three-dimensional Eulerian acid deposition model: Physical concepts and formulation, J. Geophys. Res.:
555   Atmos., 92, 14681-14700, https://doi.org/10.1029/JD092iD12p14681, 1987.

556   Chuang, M. T., Lee, C. T., Chou, C. C. K., Lin, N. H., Sheu, G. R., Wang, J. L., Chang, S. C., Wang, S. H.*, et al.*:
557   Carbonaceous aerosols in the air masses transported from Indochina to Taiwan: Long-term observation at
558   Mt. Lulin, Atmos. Environ., 89, 507-516, https://doi.org/10.1016/j.atmosenv.2013.11.066, 2014.

559   Chutia, L., Ojha, N., Girach, I. A., Sahu, L. K., Alvarado, L. M. A., Burrows, J. P., Pathak, B., and Bhuyan, P. K.:
560   Distribution of volatile organic compounds over Indian subcontinent during winter: WRF-chem simulation
561   versus observations, Environ. Pollut., 252, 256-269, https://doi.org/10.1016/j.envpol.2019.05.097, 2019.

562   Collatz, G. J., Ball, J. T., Grivet, C., and Berry, J. A.: Physio-logical and Environmental-Regulation of Stomatal
563   Conductance, Photosynthesis and Transpiration – a Model That Includes a Laminar Boundary-Layer, Agric.
564   For. Meteorol., 54, 107-136, https://doi.org/10.1016/0168-1923(91)90002-8, 1991.

565   Coppola, E., Poulton, M., Charles, E., Dustman, J., and Szidarovszky, F.: Application of Artificial Neural
566   Networks to Complex Groundwater Management Problems, Nat. Resour. Res., 12, 303-320,
567   https://doi.org/10.1023/B:NARR.0000007808.11860.7e, 2003.

568   Dickinson, R. E., Errico, R. M., Giorgi, F., and Bates, G. T.: A Regional Climate Model for the Western
569   United-States, Clim. Change, 15, 383-422, https://doi.org/10.1007/BF00240465, 1989.

570   Dunne, J. P., Horowitz, L. W., Adcroft, A. J., Ginoux, P., Held, I. M., John, J. G., Krasting, J. P., Malyshev, S.*, et*
571   *al.*: The GFDL Earth System Model Version 4.1 (GFDL-ESM 4.1): Overall Coupled Model Description
572   and Simulation Characteristics, J. Adv. Model. Earth Syst., 12, e2019MS002015,
573   https://doi.org/ARTNe2019MS00201510.1029/2019MS002015, 2020.

574   Emmons, L. K., Walters, S., Hess, P. G., Lamarque, J. F., Pfister, G. G., Fillmore, D., Granier, C., Guenther, A.*,*
575   *et al.*: Description and evaluation of the Model for Ozone and Related chemical Tracers, version 4
576   (MOZART-4), Geosci. Model Dev., 3, 43-67, https://doi.org/10.5194/gmd-3-43-2010, 2010.

577   Farquhar, G. D., Caemmerer, S. V., and Berry, J. A.: A biochemical model of photosynthetic CO_2 assimilation in
578   leaves of C3 species, Planta, 149, 78-90, https://doi.org/10.1007/BF00386231, 1980.

579   Fiore, A. M., Naik, V., and Leibensperger, E. M.: Air Quality and Climate Connections, J. Air Waste Manage.

Assoc., 65, 645-685, https://doi.org/10.1080/10962247.2015.1040526, 2015.

Fiore, A. M., Naik, V., Spracklen, D. V., Steiner, A., Unger, N., Prather, M., Bergmann, D., Cameron-Smith, P. J., *et al.*: Global air quality and climate, Chem. Soc. Rev., 41, 6663-6683, https://doi.org/10.1039/c2cs35095e, 2012.

Forkel, M., Carvalhais, N., Rodenbeck, C., Keeling, R., Heimann, M., Thonicke, K., Zaehle, S., and Reichstein, M.: Enhanced seasonal CO_2 exchange caused by amplified plant productivity in northern ecosystems, Science, 351, 696-699, https://doi.org/10.1126/science.aac4971, 2016.

Gao, Y. M., Zhuang, B. L., Wang, T. J., Chen, H. M., Li, S., Wei, W., Lin, H. J., and Li, M. M.: Climatic-Environmental Effects of Aerosols and Their Sensitivity to Aerosol Mixing States in East Asia in Winter, Remote Sens., 14, 3539, https://doi.org/10.3390/rs14153539, 2022.

Gery, M. W., Whitten, G. Z., Killus, J. P., and Dodge, M. C.: A Photochemical Kinetics Mechanism for Urban and Regional Scale Computer Modeling, J. Geophys. Res.: Atmos., 94, 12925-12956, https://doi.org/10.1029/JD094iD10p12925, 1989.

Giorgi, F.: Simulation of Regional Climate Using a Limited Area Model Nested in a General-Circulation Model, J. Clim., 3, 941-963, https://doi.org/10.1175/1520-0442(1990)003<0941:Sorcua>2.0.Co;2, 1990.

Giorgi, F. and Bates, G. T.: The Climatological Skill of a Regional Model over Complex Terrain, Mon. Weather Rev., 117, 2325-2347, https://doi.org/10.1175/1520-0493(1989)117<2325:TCSOAR>2.0.CO;2, 1989.

Giorgi, F. and Mearns, L. O.: Introduction to special section: Regional climate modeling revisited, J. Geophys. Res.: Atmos., 104, 6335-6352, https://doi.org/10.1029/98jd02072, 1999.

Giorgi, F., Marinucci, M. R., Bates, G. T., and Decanio, G.: Development of a Second-Generation Regional Climate Model (RegCM2). Part II: Convective Processes and Assimilation of Lateral Boundary Conditions, Mon. Weather Rev., 121, 2814-2832, https://doi.org/10.1175/1520-0493(1993)121<2814:Doasgr>2.0.Co;2, 1993.

Giorgi, F., Pal, J. S., Bi, X., Sloan, L., Elguindi, N., and Solmon, F.: Introduction to the TAC special issue: The RegCNET network, Theor. Appl. Climatol., 86, 1-4, https://doi.org/10.1007/s00704-005-0199-z, 2006.

Giorgi, F., Coppola, E., Solmon, F., Mariotti, L., Sylla, M. B., Bi, X., Elguindi, N., Diro, G. T., *et al.*: RegCM4: model description and preliminary tests over multiple CORDEX domains, Clim. Res., 52, 7-29, https://doi.org/10.3354/cr01018, 2012.

Guenther, A., Hewitt, C. N., Erickson, D., Fall, R., Geron, C., Graedel, T., Harley, P., Klinger, L., *et al.*: A Global-Model of Natural Volatile Organic-Compound Emissions, J. Geophys. Res.: Atmos., 100, 8873-8892, https://doi.org/10.1029/94jd02950, 1995.

Han, Z. W., Li, J. W., Xia, X. G., and Zhang, R. J.: Investigation of direct radiative effects of aerosols in dust storm season over East Asia with an online coupled regional climate-chemistry-aerosol model, Atmos. Environ., 54, 688-699, https://doi.org/10.1016/j.atmosenv.2012.01.041, 2012.

Han, Z. W., Xie, Z. X., Wang, G. H., Zhang, R. J., and Tao, J.: Modeling organic aerosols over east China using a volatility basis-set approach with aging mechanism in a regional air quality model, Atmos. Environ., 124, 186-198, https://doi.org/10.1016/j.atmosenv.2015.05.045, 2016.

He, M. Z., Kimball, J. S., Maneta, M. P., Maxwell, B. D., Moreno, A., Begueria, S., and Wu, X. C.: Regional Crop Gross Primary Productivity and Yield Estimation Using Fused Landsat-MODIS Data, Remote Sens., 10, 372, https://doi.org/10.3390/rs10030372, 2018.

Hong, C. P., Zhang, Q., Zhang, Y., Davis, S. J., Tong, D., Zheng, Y. X., Liu, Z., Guan, D. B., *et al.*: Impacts of climate change on future air quality and human health in China, Proc. Natl. Acad. Sci. U.S.A., 116, 17193-17200, https://doi.org/10.1073/pnas.1812881116, 2019.

Horowitz, L. W., Walters, S., Mauzerall, D. L., Emmons, L. K., Rasch, P. J., Granier, C., Tie, X. X., Lamarque, J.

F*., et al.*: A global simulation of tropospheric ozone and related tracers: Description and evaluation of MOZART, version 2, J. Geophys. Res.: Atmos., 108, D24, https://doi.org/10.1029/2002jd002853, 2003.

Jacobson, A. R., Schuldt, K. N., Miller, J. B., Oda, T., Tans, P., Arlyn Andrews, Mund, J., Ott, L., Collatz, G. J., Aalto, T., Afshar, S., Aikin, K., Aoki, S., Apadula, F., Baier, B., Bergamaschi, P., Beyersdorf, A., Biraud, S. C., Bollenbacher, A., Miroslaw Zimnoch.: CarbonTracker CT2019B, NOAA Global Monitoring Laboratory, [data set], https://doi.org/10.25925/20201008, 2020.

Kan, H. D., Chen, R. J., and Tong, S. L.: Ambient air pollution, climate change, and population health in China, Environ. Int., 42, 10-19, https://doi.org/10.1016/j.envint.2011.03.003, 2012.

Kiehl, J. T., Hack, J. J., Bonan, G. B., Boville, B. A., Williamson, D. L., and Rasch, P. J.: The National Center for Atmospheric Research Community Climate Model: CCM3, J. Clim., 11, 1131-1149, https://doi.org/10.1175/1520-0442(1998)011<1131:Tncfar>2.0.Co;2, 1998.

Kim, K. H., Kabir, E., and Kabir, S.: A review on the human health impact of airborne particulate matter, Environ. Int., 74, 136-143, https://doi.org/10.1016/j.envint.2014.10.005, 2015.

Kou, X. X., Zhang, M. G., Peng, Z., and Wang, Y. H.: Assessment of the biospheric contribution to surface atmospheric CO_2 concentrations over East Asia with a regional chemical transport model, Adv. Atmos. Sci., 32, 287-300, https://doi.org/10.1007/s00376-014-4059-6, 2015.

Lamarque, J. F., Dentener, F., McConnell, J., Ro, C. U., Shaw, M., Vet, R., Bergmann, D., Cameron-Smith, P*., et al.*: Multi-model mean nitrogen and sulfur deposition from the Atmospheric Chemistry and Climate Model Intercomparison Project (ACCMIP): evaluation of historical and projected future changes, Atmos. Chem. Phys., 13, 7997-8018, https://doi.org/10.5194/acp-13-7997-2013, 2013.

Lan, X.: Atmospheric Carbon Dioxide Dry Air Mole Fractions from the NOAA GML Carbon Cycle Cooperative Global Air Sampling Network, 1968-2022, Version: 2023-08-28, [data set], https://doi.org/10.15138/wkgj-f215, 2023.

Lawrence, P. J. and Chase, T. N.: Representing a new MODIS consistent land surface in the Community Land Model (CLM 3.0), J. Geophys. Res.: Biogeosci., 112, G01023, https://doi.org/10.1029/2006jg000168, 2007.

Li, B., Gasser, T., Ciais, P., Piao, S., Tao, S., Balkanski, Y., Hauglustaine, D., Boisier, J.-P*., et al.*: The contribution of China's emissions to global climate forcing, Nature, 531, 357-361, https://doi.org/10.1038/nature17165, 2016a.

Li, J. W., Han, Z. W., and Xie, Z. X.: Model analysis of long-term trends of aerosol concentrations and direct radiative forcings over East Asia, Tellus B: Chem. Phys. Meteorol., 65, 20410, https://doi.org/10.3402/tellusb.v65i0.20410, 2013a.

Li, J. W., Han, Z. W., and Zhang, R. J.: Influence of aerosol hygroscopic growth parameterization on aerosol optical depth and direct radiative forcing over East Asia, Atmos. Res., 140, 14-27, https://doi.org/10.1016/j.atmosres.2014.01.013, 2014.

Li, M., Wang, T., Han, Y., Xie, M., Li, S., Zhuang, B., and Chen, P.: Modeling of a severe dust event and its impacts on ozone photochemistry over the downstream Nanjing megacity of eastern China, Atmos. Environ., 160, 107-123, https://doi.org/10.1016/j.atmosenv.2017.04.010, 2017a.

Li, M., Zhang, Q., Kurokawa, J., Woo, J. H., He, K. B., Lu, Z. F., Ohara, T., Song, Y*., et al.*: MIX: a mosaic Asian anthropogenic emission inventory under the international collaboration framework of the MICS-Asia and HTAP, Atmos. Chem. Phys., 17, 935-963, https://doi.org/10.5194/acp-17-935-2017, 2017b.

Li, S., Wang, T. J., Zhuang, B. L., and Han, Y.: Indirect radiative forcing and climatic effect of the anthropogenic nitrate aerosol on regional climate of China, Adv. Atmos. Sci., 26, 543-552, https://doi.org/10.1007/s00376-009-0543-9, 2009.

Li, S., Wang, T. J., Solmon, F., Zhuang, B. L., Wu, H., Xie, M., Han, Y., and Wang, X. M.: Impact of aerosols on regional climate in southern and northern China during strong/weak East Asian summer monsoon years, J. Geophys. Res.: Atmos., 121, 4069-4081, https://doi.org/10.1002/2015jd023892, 2016b.

Li, X. L., Liang, S. L., Yu, G. R., Yuan, W. P., Cheng, X., Xia, J. Z., Zhao, T. B., Feng, J. M., *et al.*: Estimation of gross primary production over the terrestrial ecosystems in China, Ecol. Model., 261, 80-92, https://doi.org/10.1016/j.ecolmodel.2013.03.024, 2013b.

Liu, L., Solmon, F., Vautard, R., Hamaoui-Laguel, L., Torma, C. Z., and Giorgi, F.: Ragweed pollen production and dispersion modelling within a regional climate system, calibration and application over Europe, Biogeosciences, 13, 2769-2786, https://doi.org/10.5194/bg-13-2769-2016, 2016.

Liu, Z., Deng, Z., He, G., Wang, H. L., Zhang, X., Lin, J., Qi, Y., and Liang, X.: Challenges and opportunities for carbon neutrality in China, Nat Rev Earth Env, 3, 141-155, https://doi.org/10.1038/s43017-021-00244-x, 2022.

Lu, X., Zhang, S. J., Xing, J., Wang, Y. J., Chen, W. H., Ding, D., Wu, Y., Wang, S. X., *et al.*: Progress of Air Pollution Control in China and Its Challenges and Opportunities in the Ecological Civilization Era, Engineering, 6, 1423-1431, https://doi.org/10.1016/j.eng.2020.03.014, 2020.

Lu, X. L., Chen, M., Liu, Y. L., Miralles, D. G., and Wang, F. M.: Enhanced water use efficiency in global terrestrial ecosystems under increasing aerosol loadings, Agric. For. Meteorol., 237, 39-49, https://doi.org/10.1016/j.agrformet.2017.02.002, 2017.

Ma, D., Wang, T., Wu, H., Qu, Y., Liu, J., Liu, J., Li, S., Zhuang, B., *et al.*: The effect of anthropogenic emission, meteorological factors, and carbon dioxide on the surface ozone increase in China from 2008 to 2018 during the East Asia summer monsoon season, Atmos. Chem. Phys., 23, 6525-6544, https://doi.org/10.5194/acp-23-6525-2023, 2023a.

Ma, D. Y., Wang, T. J., Xu, B. Y., Song, R., Gao, L. B., Chen, H. M., Ren, X. J., Li, S., *et al.*: The mutual interactions among ozone, fine particulate matter, and carbon dioxide on summer monsoon climate in East Asia, Atmos. Environ., 299, 119668, https://doi.org/10.1016/j.atmosenv.2023.119668, 2023b.

Madani, N., Kimball, J. S., Affleck, D. L. R., Kattge, J., Graham, J., van Bodegom, P. M., Reich, P. B., and Running, S. W.: Improving ecosystem productivity modeling through spatially explicit estimation of optimal light use efficiency, J. Geophys. Res.: Biogeosci., 119, 1755-1769, https://doi.org/10.1002/2014jg002709, 2014.

Madronich, S. and Flocke, S.: The Role of Solar Radiation in Atmospheric Chemistry, in: Environmental Photochemistry, edited by: Boule, P., The Handbook of Environmental Chemistry, Springer Berlin Heidelberg, 1-26, https://doi.org/10.1007/978-3-540-69044-3_1, 1999.

NASA/LARC/SD/ASDC: CERES and GEO-Enhanced TOA, Within-Atmosphere and Surface Fluxes, Clouds and Aerosols Monthly Terra-Aqua Edition4A, NASA Langley Atmospheric Science Data Center DAAC, [data set], https://doi.org/10.5067/TERRA+AQUA/CERES/SYN1DEGMONTH_L3.004A, 2017.

Niinemets, Ü., Tenhunen, J. D., Harley, P. C., and Steinbrecher, R.: A model of isoprene emission based on energetic requirements for isoprene synthesis and leaf photosynthetic properties for Liquidambar and Quercus, Plant, Cell & Environment, 22, 1319-1335, https://doi.org/10.1046/j.1365-3040.1999.00505.x, 2002.

Oleson, K. W., Niu, G. Y., Yang, Z. L., Lawrence, D. M., Thornton, P. E., Lawrence, P. J., Stockli, R., Dickinson, R. E., *et al.*: Improvements to the Community Land Model and their impact on the hydrological cycle, J. Geophys. Res.: Biogeosci., 113, G01021, https://doi.org/10.1029/2007jg000563, 2008.

Pacifico, F., Harrison, S. P., Jones, C. D., Arneth, A., Sitch, S., Weedon, G. P., Barkley, M. P., Palmer, P. I., et al.: Evaluation of a photosynthesis-based biogenic isoprene emission scheme in JULES and simulation of

isoprene emissions under present-day climate conditions, Atmos. Chem. Phys., 11, 4371-4389, https://doi.org/10.5194/acp-11-4371-2011, 2011.

Pal, J. S., Giorgi, F., Bi, X. Q., Elguindi, N., Solmon, F., Gao, X. J., Rauscher, S. A., Francisco, R*., et al.*: Regional climate modeling for the developing world - The ICTP RegCM3 and RegCNET, Bull. Am. Meteorol. Soc., 88, 1395-1410, https://doi.org/10.1175/Bams-88-9-1395, 2007.

Peters, W., Jacobson, A. R., Sweeney, C., Andrews, A. E., Conway, T. J., Masarie, K., Miller, J. B., Bruhwiler, L. M. P*., et al.*: An atmospheric perspective on North American carbon dioxide exchange: CarbonTracker, Proc. Natl. Acad. Sci. U.S.A., 104, 18925-18930, https://doi.org/10.1073/pnas.0708986104, 2007.

Pu, X., Wang, T. J., Huang, X., Melas, D., Zanis, P., Papanastasiou, D. K., and Poupkou, A.: Enhanced surface ozone during the heat wave of 2013 in Yangtze River Delta region, China, Sci. Total Environ., 603, 807-816, https://doi.org/10.1016/j.scitotenv.2017.03.056, 2017.

Reynolds, R. W., Rayner, N. A., Smith, T. M., Stokes, D. C., and Wang, W. Q.: An improved in situ and satellite SST analysis for climate, J. Clim., 15, 1609-1625, https://doi.org/10.1175/1520-0442(2002)015<1609:Aiisas>2.0.Co;2, 2002.

Running, S. W.: A Measurable Planetary Boundary for the Biosphere, Science, 337, 1458-1459, https://doi.org/10.1126/science.1227620, 2012.

Running, S., Mu, Q., Zhao, M.: MOD17A2H MODIS/Terra Gross Primary Productivity 8-Day L4 Global 500m SIN Grid V006, NASA EOSDIS Land Processes Distributed Active Archive Center, [data set], https://doi.org/10.5067/MODIS/MOD17A2H.006, 2015.

Scheuch, M., Hoper, D., and Beer, M.: RIEMS: a software pipeline for sensitive and comprehensive taxonomic classification of reads from metagenomics datasets, BMC Bioinf., 16, 69, https://doi.org/10.1186/s12859-015-0503-6, 2015.

Shalaby, A., Zakey, A. S., Tawfik, A. B., Solmon, F., Giorgi, F., Stordal, F., Sillman, S., Zaveri, R. A*., et al.*: Implementation and evaluation of online gas-phase chemistry within a regional climate model (RegCM-CHEM4), Geosci. Model Dev., 5, 741-760, https://doi.org/10.5194/gmd-5-741-2012, 2012.

Shindell, D. T., Lamarque, J. F., Schulz, M., Flanner, M., Jiao, C., Chin, M., Young, P. J., Lee, Y. H*., et al.*: Radiative forcing in the ACCMIP historical and future climate simulations, Atmos. Chem. Phys., 13, 2939-2974, https://doi.org/10.5194/acp-13-2939-2013, 2013.

Sitch, S., Cox, P. M., Collins, W. J., and Huntingford, C.: Indirect radiative forcing of climate change through ozone effects on the land-carbon sink, Nature, 448, 791-795, https://doi.org/10.1038/nature06059, 2007.

Slingo, A.: A Gcm Parameterization for the Shortwave Radiative Properties of Water Clouds, J. Atmos. Sci., 46, 1419-1427, https://doi.org/10.1175/1520-0469(1989)046<1419:Agpfts>2.0.Co;2, 1989.

Small, E. E., Sloan, L. C., Hostetler, S., and Giorgi, F.: Simulating the water balance of the Aral Sea with a coupled regional climate-lake model, J. Geophys. Res.: Atmos., 104, 6583-6602, https://doi.org/Doi 10.1029/98jd02348, 1999.

Solmon, F., Elguindi, N., and Mallet, M.: Radiative and climatic effects of dust over West Africa, as simulated by a regional climate model, Clim. Res., 52, 97-113, https://doi.org/10.3354/cr01039, 2012.

Solmon, F., Giorgi, F., and Liousse, C.: Aerosol modelling for regional climate studies: application to anthropogenic particles and evaluation over a European/African domain, Tellus B: Chem. Phys. Meteorol., 58, 51-72, https://doi.org/10.1111/j.1600-0889.2005.00155.x, 2006.

Spitters, C. J. T., Toussaint, H., and Goudriaan, J.: Separating the diffuse and direct component of global radiation and its implications for modeling canopy photosynthesis Part I. Components of incoming radiation, Agric. For. Meteorol., 38, 217-229, https://doi.org/10.1016/0168-1923(86)90060-2, 1986.

Strada, S. and Unger, N.: Potential sensitivity of photosynthesis and isoprene emission to direct radiative effects

of atmospheric aerosol pollution, Atmos. Chem. Phys., 16, 4213-4234, https://doi.org/10.5194/acp-16-4213-2016, 2016.

Turuncoglu, U. U., Dalfes, N., Murphy, S., and DeLuca, C.: Toward self-describing and workflow integrated Earth system models: A coupled atmosphere-ocean modeling system application, Environ. Model. Software, 39, 247-262, https://doi.org/10.1016/j.envsoft.2012.02.013, 2013.

Wang, T., Xue, L. K., Brimblecombe, P., Lam, Y. F., Li, L., and Zhang, L.: Ozone pollution in China: A review of concentrations, meteorological influences, chemical precursors, and effects, Sci. Total Environ., 575, 1582-1596, https://doi.org/10.1016/j.scitotenv.2016.10.081, 2017.

Wang, T. J., Li, S., Shen, Y., Deng, J. J., and Xie, M.: Investigations on direct and indirect effect of nitrate on temperature and precipitation in China using a regional climate chemistry modeling system, J. Geophys. Res.: Atmos., 115, D00K26, https://doi.org/10.1029/2009jd013264, 2010.

Wang, T., Xie, M., Gao, L., and Yang, H.: Development and Preliminary Application of a Coupled Regional Climate-Chemistry Model System, J. Nanjing Univ., 40, 711-727, 2004.

Wang, T. J., Zhuang, B. L., Li, S., Liu, J., Xie, M., Yin, C. Q., Zhang, Y., Yuan, C., et al.: The interactions between anthropogenic aerosols and the East Asian summer monsoon using RegCCMS, J. Geophys. Res.: Atmos., 120, 5602-5621, https://doi.org/10.1002/2014jd022877, 2015.

Wesely, M. L.: Parameterization of Surface Resistances to Gaseous Dry Deposition in Regional-Scale Numerical-Models, Atmos. Environ., 23, 1293-1304, https://doi.org/10.1016/0004-6981(89)90153-4, 1989.

Wiedinmyer, C., Akagi, S. K., Yokelson, R. J., Emmons, L. K., Al-Saadi, J. A., Orlando, J. J., and Soja, A. J.: The Fire INventory from NCAR (FINN): a high resolution global model to estimate the emissions from open burning, Geosci. Model Dev., 4, 625-641, https://doi.org/10.5194/gmd-4-625-2011, 2011.

Xie, N., Wang, T., and Xie, X.: RegCM-Chem-YIBs: RegCM-Chem-YIBs_v1.0, Zenodo [code], https://doi.org/10.5281/zenodo.8186164, 2023.

Xie, N: CNEMC ozone and fine particulate matter site monitoring data, Zenodo [data set], https://doi.org/10.5281/zenodo.10792015, 2024.

Xie, X. D., Wang, T. J., Yue, X., Li, S., Zhuang, B. L., and Wang, M. H.: Effects of atmospheric aerosols on terrestrial carbon fluxes and CO_2 concentrations in China, Atmos. Res., 237, 104859, https://doi.org/10.1016/j.atmosres.2020.104859, 2020.

Xie, X. D., Wang, T. J., Yue, X., Li, S., Zhuang, B. L., Wang, M. H., and Yang, X. Q.: Numerical modeling of ozone damage to plants and its effects on atmospheric CO_2 in China, Atmos. Environ., 217, https://doi.org/10.1016/j.atmosenv.2019.116970, 2019.

Xiong, Z., Fu, C. B., and Yan, X. D.: Regional integrated environmental model system and its simulation of East Asia summer monsoon, Chin. Sci. Bull., 54, 4253-4261, https://doi.org/10.1007/s11434-009-0669-2, 2009.

Xu, B. Y., Wang, T. J., Ma, D. Y., Song, R., Zhang, M., Gao, L. B., Li, S., Zhuang, B. L., et al.: Impacts of regional emission reduction and global climate change on air quality and temperature to attain carbon neutrality in China, Atmos. Res., 279, 106384, https://doi.org/10.1016/j.atmosres.2022.106384, 2022.

Xu, B. Y., Wang, T. J., Gao, L. B., Ma, D. Y., Song, R., Zhao, J., Yang, X. G., Li, S., et al.: Impacts of meteorological factors and ozone variation on crop yields in China concerning carbon neutrality objectives in 2060, Environ. Pollut., 317, 120715, https://doi.org/10.1016/j.envpol.2022.120715, 2023.

Yahya, K., Wang, K., Campbell, P., Chen, Y., Glotfelty, T., He, J., Pirhalla, M., and Zhang, Y.: Decadal application of WRF/Chem for regional air quality and climate modeling over the U.S. under the representative concentration pathways scenarios. Part 1: Model evaluation and impact of downscaling, Atmos. Environ., 152, 562-583, https://doi.org/10.1016/j.atmosenv.2016.12.029, 2017.

Yin, C. Q., Wang, T. J., Solmon, F., Mallet, M., Jiang, F., Li, S., and Zhuang, B. L.: Assessment of direct

radiative forcing due to secondary organic aerosol over China with a regional climate model, Tellus Series B-Chemical and Physical Meteorology, 67, 24634, https://doi.org/10.3402/tellusb.v67.24634, 2015.

Yin, J. F., Wang, D. H., Zhai, G. Q., and Xu, H. B.: An investigation into the relationship between liquid water content and cloud number concentration in the stratiform clouds over north China, Atmos. Res., 139, 137-143, https://doi.org/10.1016/j.atmosres.2013.12.004, 2014.

Young, P. J., Archibald, A. T., Bowman, K. W., Lamarque, J. F., Naik, V., Stevenson, D. S., Tilmes, S., Voulgarakis, A*., et al.*: Pre-industrial to end 21st century projections of tropospheric ozone from the Atmospheric Chemistry and Climate Model Intercomparison Project (ACCMIP), Atmos. Chem. Phys., 13, 2063-2090, https://doi.org/10.5194/acp-13-2063-2013, 2013.

Yue, X. and Unger, N.: The Yale Interactive terrestrial Biosphere model version 1.0: description, evaluation and implementation into NASA GISS ModelE2, Geosci. Model Dev., 8, 2399-2417, https://doi.org/10.5194/gmd-8-2399-2015, 2015.

Yue, X. and Unger, N.: Aerosol optical depth thresholds as a tool to assess diffuse radiation fertilization of the land carbon uptake in China, Atmos. Chem. Phys., 17, 1329-1342, https://doi.org/10.5194/acp-17-1329-2017, 2017.

Yue, X., Strada, S., Unger, N., and Wang, A. H.: Future inhibition of ecosystem productivity by increasing wildfire pollution over boreal North America, Atmos. Chem. Phys., 17, 13699-13719, https://doi.org/10.5194/acp-17-13699-2017, 2017.

Zakey, A. S., Solmon, F., and Giorgi, F.: Implementation and testing of a desert dust module in a regional climate model, Atmos. Chem. Phys., 6, 4687-4704, https://doi.org/10.5194/acp-6-4687-2006, 2006.

Zaveri, R. A. and Peters, L. K.: A new lumped structure photochemical mechanism for large-scale applications, J. Geophys. Res.: Atmos., 104, 30387-30415, https://doi.org/10.1029/1999jd900876, 1999.

Zhang, H., Jing, X., and Li, J.: Application and evaluation of a new radiation code under McICA scheme in BCC_AGCM2.0.1, Geosci. Model Dev., 7, 737-754, https://doi.org/10.5194/gmd-7-737-2014, 2014.

Zhang, H., Wang, Z. L., Wang, Z. Z., Liu, Q. X., Gong, S. L., Zhang, X. Y., Shen, Z. P., Lu, P*., et al.*: Simulation of direct radiative forcing of aerosols and their effects on East Asian climate using an interactive AGCM-aerosol coupled system, Clim. Dyn., 38, 1675-1693, https://doi.org/10.1007/s00382-011-1131-0, 2012.

Zheng, B., Tong, D., Li, M., Liu, F., Hong, C. P., Geng, G. N., Li, H. Y., Li, X*., et al.*: Trends in China's anthropogenic emissions since 2010 as the consequence of clean air actions, Atmos. Chem. Phys., 18, 14095-14111, https://doi.org/10.5194/acp-18-14095-2018, 2018.

Zhou, Y., Huang, A. N., Jiang, J., and La, M. K.: Modeled interaction between the subseasonal evolving of the East Asian summer monsoon and the direct effect of anthropogenic sulfate, J. Geophys. Res.: Atmos., 119, 1993-2016, https://doi.org/10.1002/2013jd020612, 2014.

Zhuang, B. L., Jiang, F., Wang, T. J., Li, S., and Zhu, B.: Investigation on the direct radiative effect of fossil fuel black-carbon aerosol over China, Theor. Appl. Climatol., 104, 301-312, https://doi.org/10.1007/s00704-010-0341-4, 2011.

Zhuang, B. L., Li, S., Wang, T. J., Deng, J. J., Xie, M., Yin, C. Q., and Zhu, J. L.: Direct radiative forcing and climate effects of anthropogenic aerosols with different mixing states over China, Atmos. Environ., 79, 349-361, https://doi.org/10.1016/j.atmosenv.2013.07.004, 2013.

Zhuang, B. L., Li, S., Wang, T. J., Liu, J., Chen, H. M., Chen, P. L., Li, M. M., and Xie, M.: Interaction between the Black Carbon Aerosol Warming Effect and East Asian Monsoon Using RegCM4, J. Clim., 31, 9367-9388, https://doi.org/10.1175/Jcli-D-17-0767.1, 2018.